(Nd/Pr)2NiO4+δ: reaction intermediates and redox behavior explored by in situ neutron powder diffraction during electrochemical oxygen intercalation

Monica Ceretti, Olivia Wahyudi, Gilles André, Martin Meven, Antoine Villesuzanne, Werner Paulus

$(Nd/Pr)_2NiO_{4+\delta}$: reaction intermediates and redox behavior explored by *in situ* neutron powder diffraction during electrochemical oxygen intercalation

Monica Ceretti[a,*], *Olivia Wahyudi*[a,b], *Gilles André*[c], *Martin Meven*[d], *Antoine Villesuzanne*[b] *and Werner Paulus*[a]

a. Institut Charles Gerhardt Montpellier, UMR 5253 CNRS-UM-ENSCM, Université de Montpellier, Place Eugène Bataillon, 34095 Montpellier Cedex 5, France.

b. CNRS, Université de Bordeaux, ICMCB, UMR5026, 87 Av. Dr. A. Schweitzer, 33608 Pessac Cedex, France

c. Laboratoire Léon Brillouin, UMR12, CEA-CNRS, CEA Saclay, 91191 Gif Sur Yvette, France

d. Institute of Crystallography, RWTH Aachen University and Jülich Centre for Neutron Science (JCNS) at Heinz Maier-Leibnitz Zentrum (MLZ), 85747 Garching, Germany

ABSTRACT. Oxygen intercalation/deintercalation in $Pr_2NiO_{4+\delta}$ and $Nd_2NiO_{4+\delta}$ was followed by *in situ* neutron powder diffraction during electrochemical oxidation/reduction, in a dedicated reaction cell at room temperature. For both systems three phases, all showing the same line-width, were identified. The starting phases, $Pr_2NiO_{4.23}$ and $Nd_2NiO_{4.24}$, considered with an average orthorhombic *Fmmm* symmetry, although both show a slight monoclinic distortion, get reduced in a 2-phase reaction step to tetragonal intermediate phases with $0.07 \leq \delta \leq 0.10$ and $P4_2/ncm$ space group, which on further reduction transform, again in a 2-phase reaction step, towards the respective stoichiometric $(Pr/Nd)_2NiO_{4.0}$ phases, with *Bmab* space group. Electrochemical oxidation does, however, not proceed fully reversibly for both cases: while the re-oxidation of $Nd_2NiO_{4+\delta}$ is limited to the tetragonal intermediate phase with $\delta = 0.10$, the homologous $Pr_2NiO_{4+\delta}$ can be re-oxidized up to $\delta = 0.17$, showing orthorhombic symmetry. For the intermediate tetragonal phase, we were able to establish for $Pr_2NiO_{4.09}$ a complex anharmonic displacement behavior of the apical oxygen atoms, as analyzed by single crystal neutron diffraction and Maximum Entropy Analysis, in agreement with a low-T diffusion pathway for oxygen ions, activated by lattice dynamics.

KEYWORDS. Non-Stoichiometric Oxides, *in-situ*, neutron diffraction, electrochemistry, oxygen ionic conductors, Ruddlesden-Popper oxides.

1. Introduction

$Pr_2NiO_{4+\delta}$ (PNO) and $Nd_2NiO_{4+\delta}$ (NNO) adopt the K_2NiF_4 structure-type (Figure 1) and are today among the most promising candidates for oxygen membranes or electrolytes in solid oxide fuel cells (SOFCs), as they show high oxygen ion mobility at already moderate temperatures.[1-3]

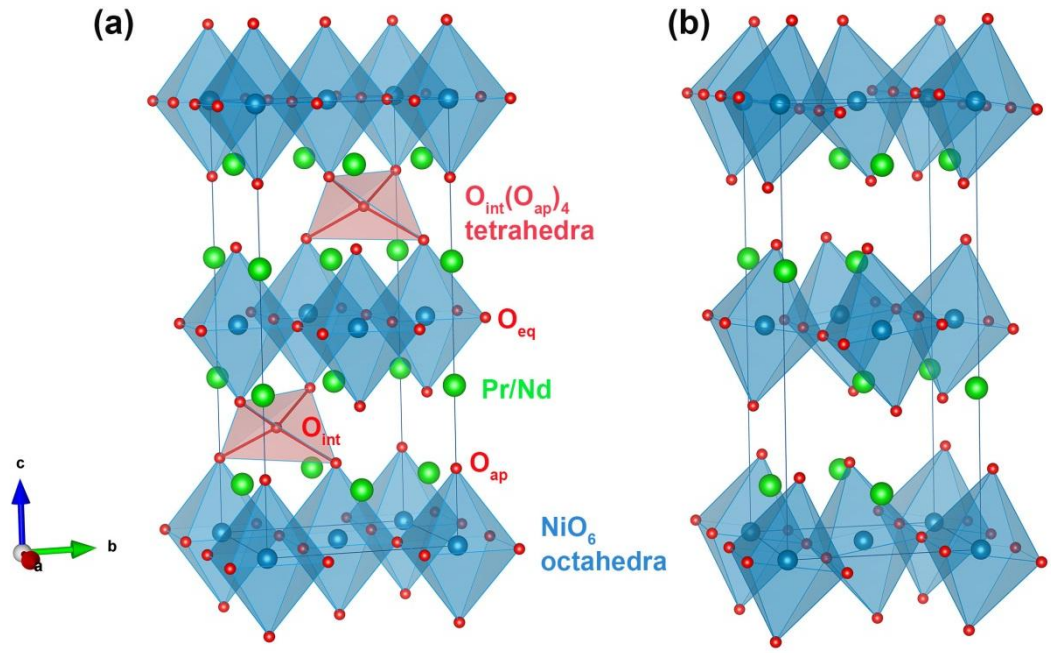

Figure 1. Crystal structures of $(Pr/Nd)_2NiO_{4+\delta}$. (a) The orthorhombic average *Fmmm* structure for $\delta \approx 0.23$, showing the interstitial (O_{int}), the apical (O_{ap}) and the equatorials (O_{eq}) oxygens. For the idealized stoichiometry corresponding to $\delta = 0.25$, one tetrahedra out of eight is occupied. (b) the stoichiometric phase with $\delta \approx 0.00$ and orthorhombic symmetry in *Bmab*

Combining inelastic neutron scattering together with first-principles lattice dynamical simulations, we have recently shown the capability of the apical oxygen atoms to diffuse towards the interstitial sites down to ambient temperature in $Nd_2NiO_{4+\delta,}$ following an energetically shallow oxygen diffusion pathway.[4] For both title compounds, NNO and PNO, we could evidence a large and anharmonic displacement behaviour of the apical oxygen atoms, suggesting a strong impact of lattice dynamics on the diffusion mechanism, which is supposed to be phonon assisted .[5, 6] This type of diffusion mechanism requires the presence of interstitial oxygen atoms, which not only induce strong local deformations of the $O_{int}(O_{ap})_4$ tetrahedra, but also, as a

consequence, push the apical oxygen atoms towards adjacent interstitial sites.[7-10] For PNO, with $\delta \approx 0.23$, the ortho/tetragonal phase transformation at around 365°C, induces the rock salt type Pr_2O_2 layer to become wholly anharmonic, showing a double well potential for the apical oxygen and the Pr atoms. This anharmonic behaviour thus naturally amplifies the highly anisotropic 2D oxygen diffusion inside the rock salt layer for these types of frameworks.

Both compounds are able to uptake important quantities on interstitial sites upon high temperature synthesis, reaching $\delta_{max.} \approx 0.23$. Together with the fact that i) interstitial oxygen atoms induce a phonon-assisted diffusion mechanism at moderate temperatures and ii) an important amount of $\delta \approx 0.15$ is still present at 1000°C, PNO and NNO reveal as obviously promising candidates for oxygen membranes operating at moderate temperature. Finally yet importantly, PNO and NNO are key candidates to explore oxygen diffusion mechanisms, triggered by low-energy phonon modes. In order to better explore the oxygen intercalation reaction mechanism at ambient conditions on both PNO and NNO, and to build the respective phase diagram as a function of the oxygen stoichiometry δ, we studied this reaction by *in situ* neutron diffraction on polycrystalline electrodes. While electrochemical oxygen intercalation has already been explored for NNO by X-ray diffraction[11], no such studies have been reported in literature for PNO. In this work, we were especially motivated to explore possible oxygen ordering in course of the intercalation reaction using *in situ* neutron diffraction, which is more sensitive to low-Z elements such as oxygen.

2. Experimental Details and Methods

Synthesis and Working Electrode Preparation. $Nd_2NiO_{4+\delta}$ and $Pr_2NiO_{4+\delta}$ were prepared by solid state reaction technique. Nd_2O_3 (heated in vacuum at 1000°C before using), Pr_6O_{11} and

NiO were thoroughly mixed together in stoichiometric quantities and heated in air at 1250°C for 12 hours. The powder was then pressed into pellets of 13 mm diameter and 1 g mass, which were again heated in air for 48 hours under the same conditions, with an intermediate regrinding and pelletizing. The as obtained pellets were used as working electrodes for the structural studies by *in situ* neutron powder diffraction (NPD). The electrochemical cell used for NPD was made of quartz, quite transparent to neutrons, containing three electrodes (one working electrode, Pt counter electrode and Ag/AgCl reference electrode) in a 1 N KOD electrolyte, as described in details elsewhere.[12] The working electrode (sample) consisted of reshaped pellets (total mass about 3 g) glued together by a carbon glue and contacted by a Pt wire. The electrolyte was prepared from equivalent amounts of 40% KOD solution in D_2O (99.9% enriched, Aldrich).

Single Crystal Growth. High quality $Pr_2NiO_{4+\delta}$ single crystals were grown by the traveling solvent floating zone method (TSFZ) as described elsewhere.[13] Compared to polycrystalline electrodes, which react on a reasonable timescale in thermodynamical equilibrium, the reactivity of centimeter-sized single crystals - used for neutron diffraction structural investigations - is strongly reduced due to the smaller active reaction surface. Therefore, in order to obtain the target oxygen stoichiometry of δ=0.1 in a reasonable reaction time, the crystals were annealed under a dynamic vacuum ($\approx 10^{-3}$ mbar) at 600°C.

Neutron Diffraction.

In situ neutron powder diffraction studies were performed on the G4.1 two-axis diffractometer of the Laboratoire Léon Brillouin in Saclay (LLB, Orphée reactor), France. The diffractometer is equipped with an 800-cells multi-detector covering a 2θ range of 80°, the used wavelength being 2.42 Å.

$Nd_2NiO_{4+\delta}$ powder diffraction patterns were collected every 2 hours during a period of 3.5 days, achieving a charge transfer of 0.01 electrons/formula unit (e^-/f.u.) per diffractogram. Due to the limitation of neutron beam time, powder patterns for $Pr_2NiO_{4+\delta}$ were recorded every hour, with a charge transfer of 0.015 e^-/f.u. per diagram. During all *in situ* experiments, fresh electrolyte was pumped at constant flow through the electrochemical cell in order to guarantee both stable reactions and a constant background during the whole experiment. All the electrochemical reduction/oxidation reactions were carried out in a galvanostatic mode, applying a constant current. The applied current density did not exceed 500 $\mu A/cm^2$. NPD experiments were performed during the reduction of the as sintered starting compounds until the stoichiometric $Nd_2NiO_{4.00}$ and $Pr_2NiO_{4.00}$ are reached. After completing the reduction, both samples were re-oxidized in order to verify the reversibility of the oxygen intercalation reaction.

Further structural investigations were performed by NPD, using the 3T2 two axes diffractometer at LLB (λ=1.225 Å), as well as single crystal neutron diffraction on the four-circle diffractometer HEiDi at MLZ in Garching, Germany (λ = 0.79 Å). Rietveld refinements of all NPD data were done using the FULLPROF suite.[14] Special care was taken for the background correction of the *in situ* diffraction experiment: it was carefully determined from the starting compound and taken as constant for the whole experiment. Single crystal refinements were carried out using SHELXL.[15] Nuclear densities have been reconstructed in real space through the maximum entropy method (MEM) via PRIMA (Practice Iterative MEM Analysis);[16] scattering lengths were taken from ref. 11, and nuclear density distributions were visualized by using the VESTA program.[17]

3. Results and Discussion

3.1 $Nd_2NiO_{4+\delta}$ electrochemical reduction-oxidation

$Nd_2NiO_{4+\delta}$ shows a rich sequence of phase transitions and distinct line phases as a function of oxygen stoichiometry (δ), even at room temperature. For $Nd_2NiO_{4+\delta}$, variation of δ can been controlled as a function of temperature and oxygen partial pressure.[18, 19] Only ref [11] reports on the structural evolution of NNO during electrochemical oxygen intercalation/deintercalation at ambient temperature, studied by *ex situ* X ray diffraction. The obtained phase diagram shows, in addition to the orthorhombic *Fmmm* starting phase, reported as $Nd_2NiO_{4.18}$, and the stoichiometric end phase $Nd_2NiO_{4.00}$, a non-stoichiometric tetragonal phase $Nd_2NiO_{4.06\pm0.02}$, which has been indexed in the tetragonal space group *F4/mmm*. However, reported lattice parameters, oxygen stoichiometry as well as symmetry, are not always consistent, showing problems with the reproducibility as well as the complexity of the system.

In the present work, neutron powder diffraction was chosen to follow the structural evolution of the title compounds, during the electrochemical reaction. Importantly, neutron diffraction yields bulk information, while the penetration depth of X-rays is limited to several μm only, rendering difficult to quantify the different volume fractions of the respective phases formed during the reaction. This is important when it comes to quantify phase analysis, which is a difficult task when analyzed with X-ray diffraction, related to inhomogeneities between the surface and in the bulk of the working electrode, especially for solid-state reactions with slow kinetics. The second advantage for neutron diffraction is that the coherent neutron scattering length of oxygen (~5.803 fm) is of the same magnitude of that for Nd/Pr (~ 7.69 fm/4.58 fm) and Ni (~ 10.3 fm), resulting in a significantly better contrast for (low-Z) oxygen atoms; this allows the detection of oxygen ordering and respective reaction intermediates.

NPD patterns of $Nd_2NiO_{4+\delta}$ measured *in situ* during a complete electrochemical reduction-oxidation cycle on the neutron diffractometer G4.1 (λ=2.42Å) are shown in Figure 2. Data were corrected for an unbalanced background, resulting essentially from the quartz cell and KOD electrolyte. The background was determined with good counting statistics for the first diffraction pattern, prior to the reduction, and subsequently subtracted from all following diffractograms. The electrochemical reaction was performed in a galvanostatic mode, allowing a direct correlation of the structural and magnetic evolution with the charge transfer, i.e. the oxygen stoichiometry (see Eq. 1). The starting compounds, $Nd_2NiO_{4+\delta}$ and $Pr_2NiO_{4+\delta}$, showing respectively an oxygen excess stoichiometry of $\delta \approx 0.24$ and $\delta \approx 0.23$, are usually reported to be orthorhombic, but reveal in fact a minor monoclinic splitting, the monoclinic angle being 90.06° and 90.07° respectively. This monoclinic distortion can already be detected on a high resolution laboratory X-ray diffractometer on a highly crystalline sample with low mosaicity. Although the used electrodes were monoclinic (space group *F112/m*, which is a subgroup of *Fmmm*) with a = 5.3681(4) Å, b = 5.4439(4)Å, c = 12.3514(10)Å, γ = 90.07(1)° for NNO and a = 5.3945(4) Å, b = 5.4538(4)Å, c = 12.4408(10)Å, γ = 90.07(1)° for PNO (see Figures S1 and S2), they are considered in the following as orthorhombic with *Fmmm* symmetry, as the instrumental resolution of the G4.1 neutron powder diffractometer did not allow discriminating between orthorhombic and monoclinic symmetry.

For the electrochemical reduction of $Nd_2NiO_{4+\delta}$ an electrode of $40 \times 10 \times 1$ mm^3 was obtained using four sintered and reshaped pellets, in order to optimize for intensities. Figure 2 (bottom) shows the obtained diffractograms as a function of the charge transfer, showing principally 3 distinct phases: (i) the orthorhombic starting phase with *Fmmm* symmetry, (ii) a tetragonal

intermediate phase with *P4$_2$/ncm* symmetry, (iii) and the fully reduced and stoichiometric phase $Nd_2NiO_{4.0}$, having the low temperature orthorhombic (LTO) phase with *Bmab* space group.

The electrochemical reaction can formally be described as:

$$RE_2NiO_{4.00} + \delta O^{2-} \leftrightarrow RE_2NiO_{4+\delta} + 2\delta e^- \qquad (1)$$

Thus the oxygen stoichiometry δ is directly related to the charge transfer (*n*), expressed in e^-/f.u., by the simple relation $\delta = 2n$. A charge transfer of about 0.48 e^-/f.u. was needed to reach the pure stoichiometric phase, corresponding to the intercalation of $\delta = 0.24$ oxygen atoms. The starting material was thus calculated to be $Nd_2NiO_{4.24}$, in agreement with the value reported in literature.[13]

All diffractograms were analyzed by Rietveld refinement using the FullProf package. Here, the refinements - and especially the identification of the different phases - are not an easy task, mainly due to the very similar lattice parameters of all present phases. Rietveld refinements for the three different phases are reported in Figure S3-S5. Since the quality of the in situ diffractograms does not allow precise occupancies and thermal displacements, and to avoid incoherent divergences in the refinements, we kept the structural models in *Fmmm*, *P4$_2$/ncm* and *Bmab* unchanged, while essentially refining the volume fraction and lattice parameters only. In this way we could obtain a reasonable approach of the phase relations during the electrochemical reactions. Refined lattice parameters and scale factors are illustrated in Figure 3(a) and 3(b), respectively, as a function of the charge transfer *n* (and thus of the oxygen stoichiometry δ).

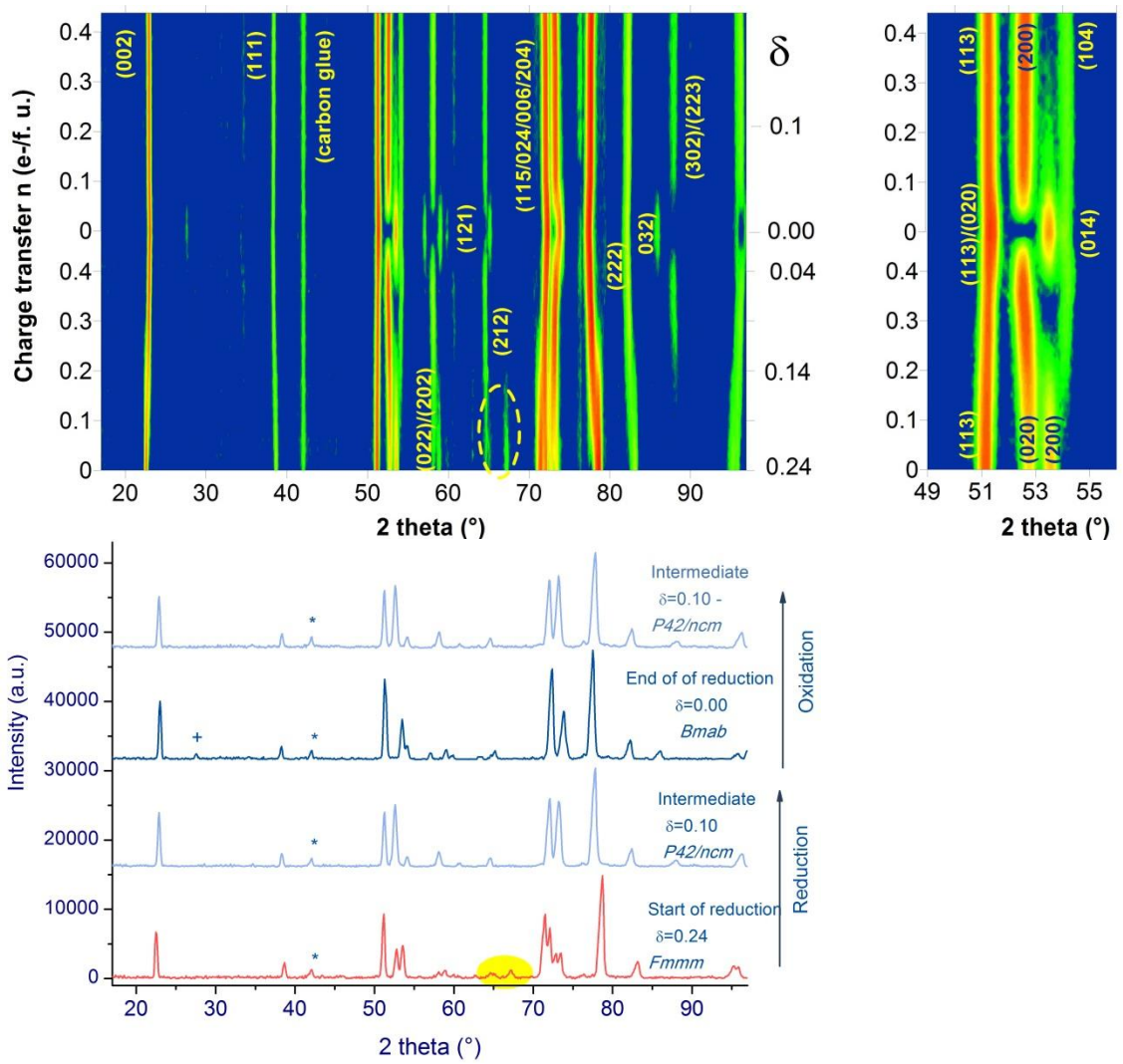

Figure 2. Evolution of the NPD patterns obtained *in situ* during the electrochemical reduction-oxidation of $Nd_2NiO_{4+\delta}$ (G41, λ = 2.422(2) Å). The yellow ellipsoid shows the incommensurate superstructure reflections of the starting compound. In the upper right part, zoom-in view of the diffraction patterns between 40° and 56° in 2θ.For comparison, the different diffraction patterns are reported in the bottom part: the pattern of the starting phase with *Fmmm* symmetry and δ = 0.24, the intermediate $P4_2/ncm$ phase with δ = 0.10 and the fully reduced stoichiometric compound with *Bmab* symmetry (δ = 0.00) as well as the maximum re-oxidized phase. Peaks indicated with (*) arise from the carbon glue, while the reflection indicated by (+), in the stoichiometric phase, is of magnetic origin, showing (011) indexation.

For the $Nd_2NiO_{4.24}$ starting phase, we observed in addition to those corresponding to the *Fmmm* space group two reflections at 2θ=65° and 67° (Figure 1). Both reflections are not detectable by X-ray diffraction, even at good counting statistics, and are supposed to be superstructure reflections, related to an incommensurate superstructure due to oxygen ordering, as already discussed in ref. [7]. While the reflection at 2θ = 67° completely disappears after a charge transfer of 0.15 e^-/f.u., the one at 2θ = 65° can be further indexed as (212) for the tetragonal and the stoichiometric $Nd_2NiO_{4.00}$ phase, for which the corresponding orthorhombic (122) reflection is absent due to the extinction rules of space group *Bmab*. A careful inspection of the lattice parameters and respective scale factors (Figure 2) reveals the starting and end phase to be both stoichiometric line phases, since their lattice parameters are constant over the whole range of the reaction and only their respective scale factors vary. Inspection of the evolution of the scale factors, identifies the transformation of the $Nd_2NiO_{4.24}$ starting phase towards the tetragonal intermediate phase as a two-phase region step (see Figure 3(b)). However, the *c* lattice parameter of the tetragonal phase is slightly but continuously decreasing, which seems somehow to be contradictory with the two-phase behavior.

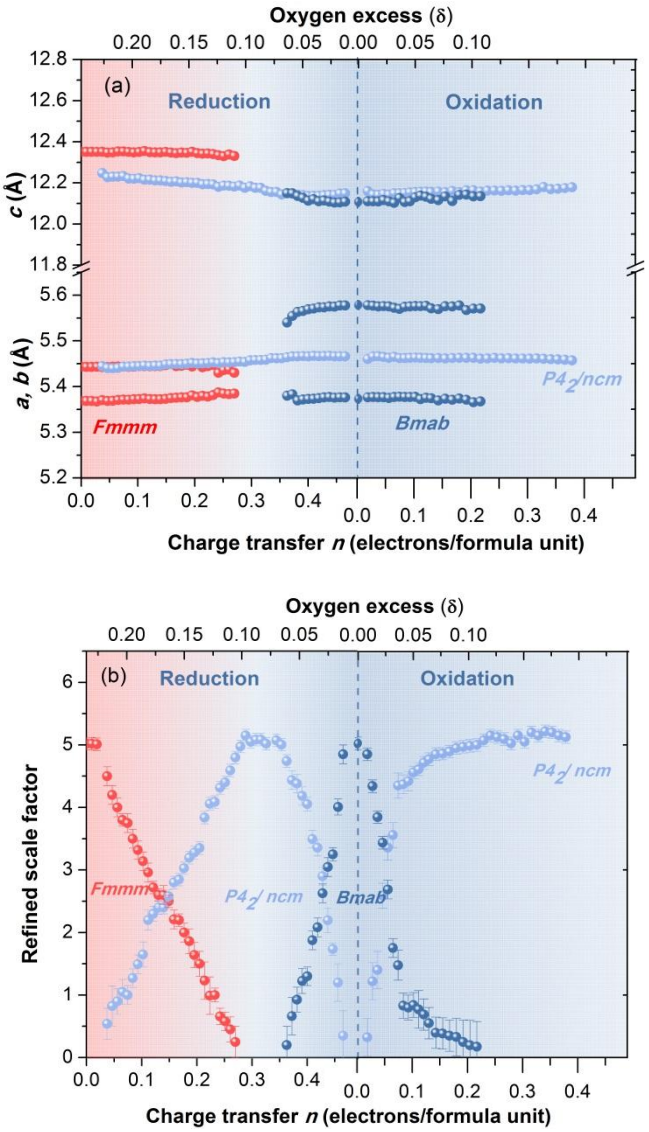

Figure 3. $Nd_2NiO_{4+\delta}$: evolution of the unit cell parameters *a, b, c*, (a) and of the refined scale factor parameter (b), as a function of the charge transfer *n* (and thus of the oxygen excess δ), obtained from Rietveld refinements. The errors bars in the *a, b, c*, parameters are within the dimensions of the dots. Refinements were done for the *Fmmm* orthorhombic starting phase (red dots), the *P4₂/ncm* tetragonal intermediate phase (light blue dots) and the stoichiometric orthorhombic phase with *Bmab* symmetry (dark blue dots). Oxygen content was derived from the electrochemical titration data.

The space group of the tetragonal intermediate phase does, however, not correspond to *F4/mmm*, as reported earlier from X-ray diffraction studies in ref. [11], but to $P4_2/ncm$, as indicated by the presence of *P*-type reflections, e.g. the (104) reflection at $2\theta = 53°$; its intensity increases linearly with the charge transfer in the beginning of the reduction, while the incommensurate reflection at 67° weakens simultaneously. The appearance of *P*-type reflections, whereas their intensity is close to zero in X ray diffraction, is an interesting observation, as all tetrahedral sites of the interstitial oxygen atoms are symmetrically equivalent for *F4/mmm*, but split into two different sites in $P4_2/ncm$, with different point symmetries. The *4b* Wyckoff site in *(¾ ¼ ¾)* shows a site symmetry of $\bar{4}$, while a *2.mm* site symmetry is obtained for the *(¼ ¼ z)* site, with *4e* Wyckoff notation. As discussed below for $Pr_2NiO_{4.09}$, only the *4b* sites are occupied by interstitial oxygen atoms. This is at first sight surprising, as a lower structural flexibility of the $O_{int}(O_{ap})_4$ tetrahedron centered at *(¾ ¼ ¾)* is expected, related to the $\bar{4}$ site symmetry and associated symmetrical increase in case of oxygen occupation (as outlined below, section 3.3), and the resulting short O_{int}-O_{ap} oxygen distances of about 2.2 Å. The situation seems, however, to be different for the *4e* position, allowing an asymmetric opening of the $(O_{ap})_4$ tetrahedron and thus enabling an easier structural response when it comes to avoid steric constraints.

In this context it is also interesting to note that thermally prepared $Nd_2NiO_{4.08}$ has been reported to show a slight deviation from the tetragonal to orthorhombic symmetry with the *Pccn* space group, as explored by X-ray diffraction.[20] While for structure refinements in ref [20] all positions of the basic structure were constraint to the equivalent positions in the $P4_2/ncm$ space group, it was not possible to conclude on the localization of interstitial oxygen atoms. The fact that the homologous $Pr_2NiO_{4.09}$ phase shows a selective occupation of the *(¾ ¼ ¾)* tetrahedral site in the

P4₂/ncm space group becomes an important finding, as a corresponding site symmetry is absent for the *Pccn* space group. This suggests that the true symmetry of $Nd_2NiO_{4.08}$ could also be the tetragonal *P4₂/ncm* rather than the postulated *Pccn*.

Following the scale factor (Figure 3(b)), we can clearly define a single-phase region for the *P4₂/ncm* phase for $0.07 \leq \delta \leq 0.10$, rendering $Nd_2NiO_{4+\delta}$ to be non-stoichiometric. Below δ = 0.07 the reduction proceeds as a two-phase reaction, where the volume fraction of $Nd_2NiO_{4.07}$ continuously decreases, while the amount of stoichiometric $Nd_2NiO_{4.00}$ accordingly increases. It goes along with a significant increase of the orthorhombicity *(a-b)/(a+b)* = 0.0182, compared to 0.0069 for the $Nd_2NiO_{4.24}$ starting phase. From Figure 2, the orthorhombic splitting of the basic reflections as (200/020) and (202/022) becomes evident, while the (212) and also the antiferromagnetic (011) reflections have no orthorhombic counterparts, as they both are forbidden by symmetry. The zoomed section from 49°-56° shows, in addition to the (200/020) splitting, the evolution of the (104) reflection, which is characteristic of the *P4₂/ncm* and the *Bmab* phases only. Refinements carried out for the nuclear/magnetic structure of $Nd_2NiO_{4.00}$ in space group *Bmab* yielded a magnetic moment of M_x = 0.686 μ_B, showing G-type antiferromagnetic ordering similar to that reported in ref. [21]

After obtaining the stoichiometric $Nd_2NiO_{4.00}$ phase, the current polarization was reversed to start the re-oxidation. As shown in the evolution of the diffraction patterns, the deintercalation/intercalation reaction turns out as not fully reversible, since the re-oxidation stops when reaching the tetragonal phase, corresponding to $Nd_2NiO_{4.10}$. Although the current density was the same as the one used during the reduction, the slope of the scale factor during re-oxidation, in the region $0 \leq n \leq 0.08$ e^-/f.u., is steeper compared to the reduction reaction. Beyond n = 0.08 e^-/f.u., a significantly reduced slope is observed, probably related to a change in

the kinetics of the oxidation reaction. A transformation from the orthorhombic $Nd_2NiO_{4.00}$ phase to the tetragonal phase is clearly accompanied by the vanishing of the splitting of orthorhombic reflections like the *(202/022)*. The separation of the strongest reflections *(200/020)* cannot easily be used for a quantitative phase identification due to the almost perfect overlap of the *(020)* reflection of the *Bmab* phase with the *(113)* reflection of both phases. Further attempts to electrochemically oxidize the tetragonal phase of $Nd_2NiO_{4+\delta}$ beyond $\delta \approx 0.09$, to access the *Fmmm* initial phase $Nd_2NiO_{4.24}$, did not succeed.

3.2 $Pr_2NiO_{4+\delta}$ electrochemical reduction-oxidation

The electrochemical reduction/oxidation of as sintered $Pr_2NiO_{4.23}$ pellets was done in the same way as described above for $Nd_2NiO_{4.24}$. Thereby, the indicated oxygen stoichiometry is the result of TG analysis, carried out under hydrogen, as well as the electrochemical titration outlined below. The diffractograms, obtained by *in situ* NPD are given in Figure 4, as a function of the charge transfer. All patterns were corrected for background as described above for NNO.

In analogy to NNO, the starting phase is orthorhombic and all reflections can be indexed in the *Fmmm* space group, except the one situated at 67.5° in 2θ which is again attributed to an incommensurate superstructure reflection. Its intensity is, however, much lower compared to NNO, as already mentioned in ref. [22]. Following the refined lattice parameters and scale factor as depicted in Figures 5(a) and 5(b), we conclude on a very similar phase diagram compared to $Nd_2NiO_{4+\delta}$. The reduction proceeds in a two-phase reaction mechanism from the orthorhombic $Pr_2NiO_{4.23}$ to the tetragonal $Pr_2NiO_{4.10}$ phase (refinement is given in Figure S6), which gets further reduced to $Pr_2NiO_{4.07}$ in a single-phase reaction mechanism. The formation of stoichiometric $Pr_2NiO_{4.00,}$ with *Bmab* space group (Figure S7), follows again a two-phase reaction mechanism. As for its homologue NNO, fully reduced $Pr_2NiO_{4.00}$ shows

antiferromagnetic G-type ordering, as deduced from the (011) reflection, the magnetic moment of Ni^{2+} pointing along the *a*-axis with $M_x = 0.550\ \mu_B$.[23, 24]

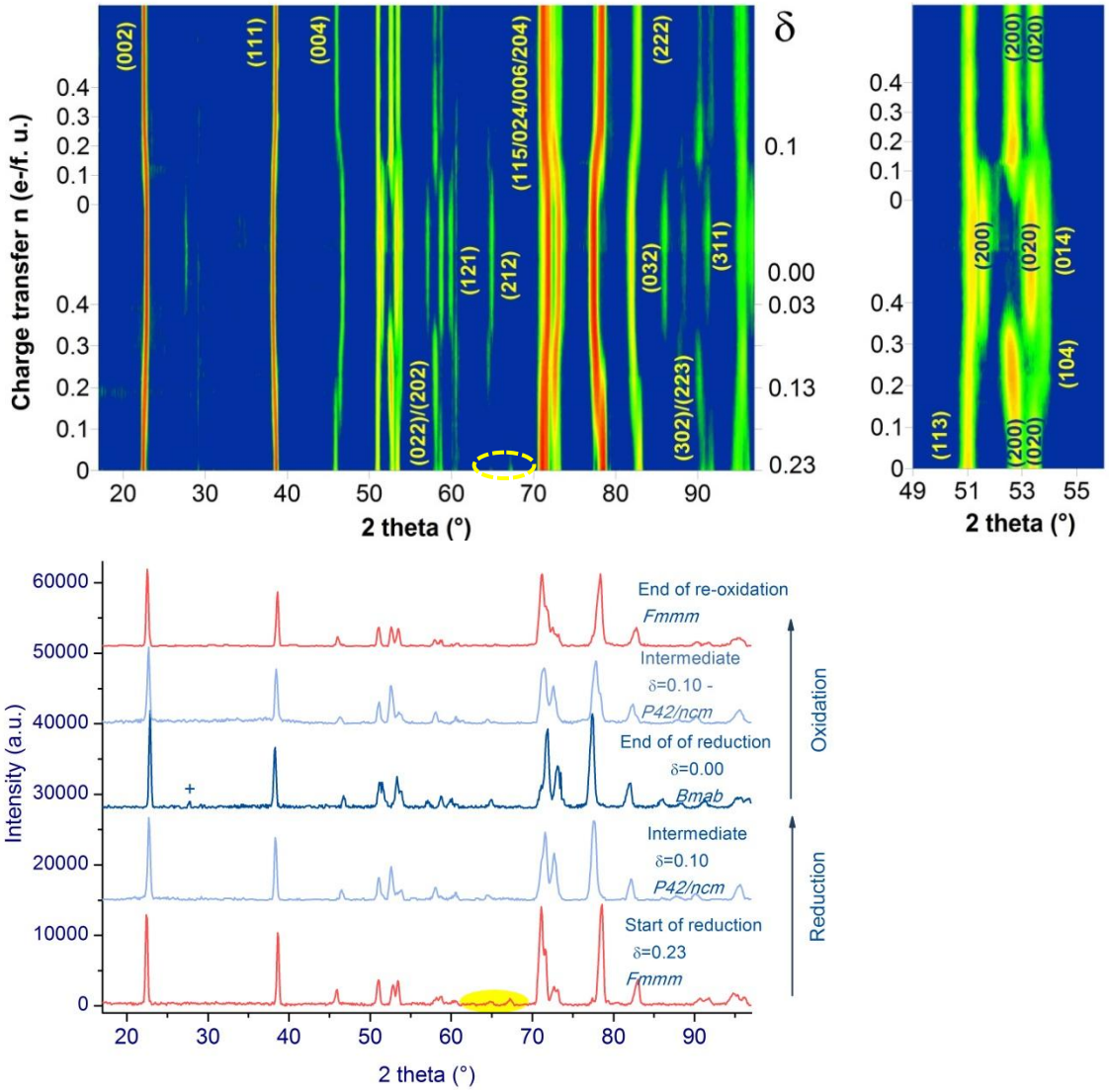

Figure 4. Evolution of the NPD patterns obtained *in situ* during the electrochemical reduction-oxidation of $Pr_2NiO_{4+\delta}$ (G41, λ = 2.422(2)Å). In the upper right part, zoom-in view of the diffraction patterns between 40° and 56° in 2θ. For comparison, the different diffraction patters are also reported in the bottom: the starting pattern *Fmmm* (δ = 0.23), the intermediate *P4₂/ncm* for δ = 0.10, the stoichiometric fully reduced compound (δ = 0.00) *Bmab*, once again the intermediate *P4₂/ncm* phase (δ = 0.10) and the final *Fmmm* phase reached upon re-oxidation. The reflection indicated by (+) in the stoichiometric phase is magnetic. The yellow ellipsoid shows the incommensurate superstructure reflections of the starting compound.

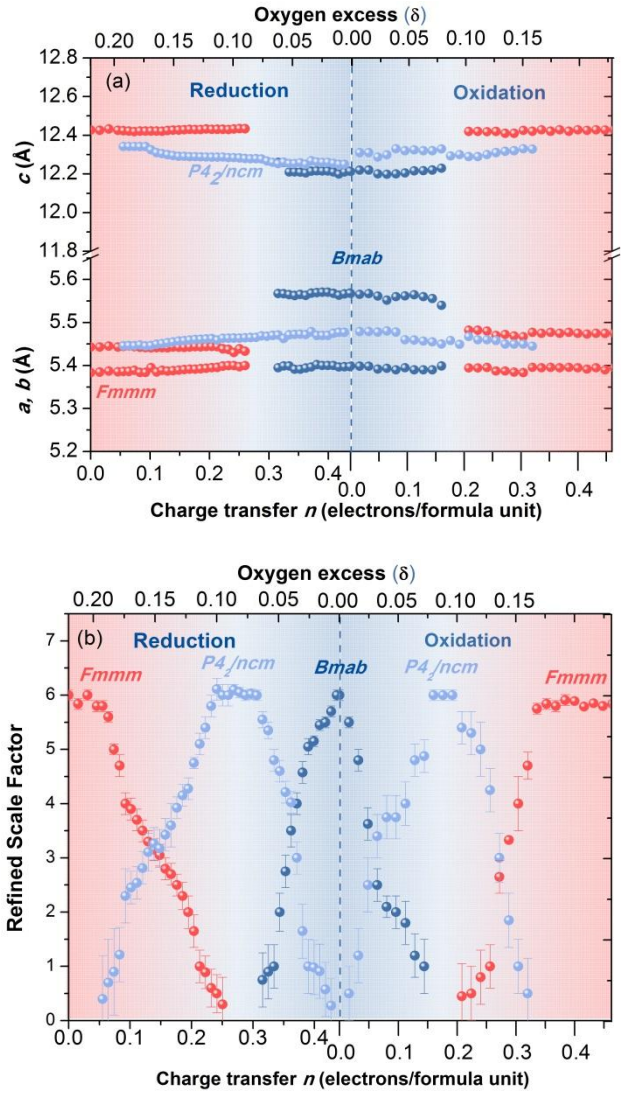

Figure 5. $Pr_2NiO_{4+\delta}$: (a) evolution of the unit cell parameters *a*, *b*, *c*, and (b) of the refined scale factor parameters as a function of the charge transfer *n* (and thus of the oxygen excess δ). The errors bars in the *a*, *b*, *c*, parameters are inside the dimensions of the dots. Refinements were done for the *Fmmm* orthorhombic starting phase (red dots), the *P4₂/ncm* tetragonal intermediate phase (light blue dots) and the stoichiometric orthorhombic *Bmab* phase (dark blue dots). Oxygen content was derived from the electrochemical titration data.

Contrary to the NNO system, the re-oxidation reaction seems at first sight to be fully reversible for PNO: the final oxidized phase shows again the *Fmmm* symmetry with the same scale factor as the starting phase. However, the phase purity during the oxidation is not so nicely defined as for the reduction, as it can be seen from the individual patterns shown in Figure 4 (bottom). This might be due, at least partially, to grain contact problems related to significant changes in the volume, i.e. lattice parameters. The evolution of the scale factors shows that the re-oxidized phase is already reached at a charge transfer equivalent to $\delta = 0.17$ only. Moreover, it does not show any incommensurate reflections, and the orthorhombicity is slightly larger compared to the starting phase, the lattice parameters being $a = 5.3945(4)$Å, $b = 5.4748(6)$Å, $c = 12.4281(8)$Å. These values, however, perfectly match with those of the $Pr_2NiO_{4.16}$ phase, prepared by classical solid state reaction, and which has been reported as a line phase with *Fmmm* symmetry.[25]

Since oxygen formation was observed at the counter electrode during the electrochemical oxidation when reaching a charge transfer corresponding to $\delta = 0.16$, it becomes evident that further oxidation towards $\delta = 0.23$ is hindered, for reasons unclear so far. We anyway counterchecked the symmetry and lattice parameters of this maximum re-oxidised phase by *ex situ* high resolution X-ray diffraction, in order to verify or not a possible monoclinic symmetry, as obtained for the starting phase $Pr_2NiO_{4.23}$ (Figure S8). Its pattern matches also here nicely with an orthorhombic *Fmmm* structure, although a significant broadening of the reflection profiles is observed, probably related to reduced mosaicity induced by the reduction/oxidation reaction. We therefore conclude that the maximum electrochemically oxidized phase shows a stoichiometry corresponding to $Pr_2NiO_{4.16}$ with *Fmmm* symmetry.

The reversibility of the reaction is clearly enhanced for PNO when comparing to the homologue NNO system, as oxidation continues far beyond the tetragonal intermediate phase. Nevertheless, a full reversibility remains incomplete for both systems. The question, whether the *Fmmm*-phase corresponding to $\delta = 0.16$ already appears during the reduction from the as sintered $Pr_2NiO_{4.23}$ electrodes, is difficult to answer, due to similarities in the lattice parameters and limited instrumental resolution. From the refinements (see Figures 5(a) and 5(b)), it can be seen that the *c*-axis and *a*-axis parameters of the re-oxidized phase are almost identical to the starting phase parameters, while the *b*-axis parameter corresponds closely to the (*a, b*)-parameter of the intermediate tetragonal phase.

Further inspections of the evolution of all *P*-type reflections, i.e. reflections that are forbidden in *Fmmm*, reveal a steady increase in their intensities from the beginning of the reduction and which go through the stoichiometry range corresponding to $\delta = 0.16$. This clearly suggests the absence of this *Fmmm* phase with $\delta = 0.16$ during the electrochemical reduction.

3.3 Intermediate tetragonal phase

As for NNO, a non-stoichiometric tetragonal phase $Pr_2NiO_{4+\delta}$ with $0.07 \leq \delta \leq 0.10$ was obtained during the electrochemical reduction/oxidation, although there is no obvious reason for this specific reaction intermediate to appear. In addition, the *$P4_2/ncm$* space group, implying an octahedral tilting around the [110] axis with respect to the *F*-cell (low temperature tetragonal - LTT - phase), usually occurs only for the low-T modification of nickelates with Ruddlesden Popper frameworks with δ close to 0, as is the case for $RE_2NiO_{4.0}$ (RE = La, Nd, Pr).[21] The formation of this LTT-type phase with a significant interstitial oxygen stoichiometry, during the electrochemical reaction at ambient temperature, is therefore surprising.

This astonishing formation of this tetragonal non-stoichiometric phase, for both $Nd_2NiO_{4+\delta}$ and $Pr_2NiO_{4+\delta}$ with $0.07 \leq \delta \leq 0.10$, motivated us to further investigate related structural changes, with a special focus on the occupation of the two non-equivalent tetrahedral sites and related oxygen ordering. To this end we first investigated the maximum electrochemically re-oxidized $Nd_2NiO_{4.09}$ sample, used for the *in situ* experiment, by high resolution powder diffraction on the 3T2 diffractometer at LLB. The refinement, which is given in the Supplementary Information (Figure S9 and Tables S1-S2), was non-conclusive with respect to a preferred occupation of the two tetrahedral sites. We checked both tetrahedral site occupation separately, and were able to refine a stoichiometry corresponding to $\delta = 0.09$ for both cases, and underlining the difficulty to differentiate between both tetrahedral sites even when neutron powder diffraction is employed. To obtain a higher structural resolution, we attempted to study the homologous PNO phase by single crystal neutron diffraction. The reaction kinetics for single crystals of suitable size is, however, strongly reduced for electrochemical reactions, and the as grown $Pr_2NiO_{4.23}$ single crystal was instead reduced for 30 minutes at 600°C and 10^{-3} mbar vacuum yielding the tetragonal phase $Pr_2NiO_{4.09}$.

Its crystal structure was subsequently investigated on HEIDI, the neutron single crystal diffractometer installed at the hot source of the FRM II reactor of MLZ. Structure factors were collected up to high q-values, i.e. up to $\sin\theta/\lambda = 0.87$ Å^{-1}. The refinements were done in the space group *P4$_2$/ncm*. No absorption correction was applied due to the negligible absorption coefficients of the compounds. The refined structural data (ShelxL) are summarized in Table 1.

Table 1. $Pr_2NiO_{4.09}$: structure data obtained from single crystal neutron diffraction data, collected on diffractometer HEiDI@MLZ with λ= 0.79 Å

Atom	x	y	z	Occ	U_{11}	U_{22}	U_{33}	U_{23}	U_{13}	U_{12}
Pr	0.9909(3)	0.9909(3)	0.3618(2)	2.00	0.0093(6)	0.0093(6)	0.0105(8)	-	-	0.0018(5)
Ni	0	0	0	1.00	0.0029(5)	0.0029(5)	0.0143(7)	0.0003(2)	0.0003(2)	-0.0004(2)
O1	¼	¼	0.9797(2)	1.00	0.0058(7)	0.0058(7)	0.019(1)	-	-	-0.0023(5)
O2	¾	¼	0	1.00	0.007(7)	0.007(7)	0.032(1)	-	-	0.0016(6)
O3	0.0380(3)	0.0380(3)	0.1772(2)	1.92(9)	0.0222(8)	0.0222(8)	0.0102(9)	0.0006(4)	0.0006(4)	-0.0065(7)
O4	¾	¼	¼	0.09(2)	0.013(2)					

Refinements were carried out in SG $P4_2/ncm$ with unit cell parameters $a = b = 5.476(9)$ Å; $c = 12.317(5)$ Å, 996 measured reflections ($\sin\theta/\lambda = 0.79$ Å^{-1}), (465 unique) R_{int}(hkl) = 2.8%, Rw=5.6%, GooF=1.23. (U_{ij} are in Å^2). The special positions (*xxz*) of Pr and O3 refer to the second setting of SG $P4_2/ncm$. The under-occupation of the equatorial O3 is probably due to part of the density "escaping" from the harmonic description.

The structure corresponds to the LTT structure-type, reported previously for different stoichiometric $RE_2MO_{4.0}$ phases at low temperature.[24] It is characterized by the tilt of the octahedra around the [110]-axis, with respect to the *F*-cell. From a difference Fourier analysis, it turns out that the interstitial oxygen atoms are located in the (4b) tetrahedral site only, in (¾ ¼ ¼), resulting into an unreasonable short distance of 2.18 Å (4x) between the O_{int} and O_{ap}. Thereby the shift of the apical oxygen atoms results in a rotation of the (4b) tetrahedra around the *c*-axis, which corresponds here to 10° (see Figure 6). As further outlined below, the short O_{int}-O_{ap} distances do not reveal the real but a more average structure approach, not taking into account the local O_{ap} displacements, induced by the presence of O_{int}. At this stage it is, however, not clear whether the better localisation of the interstitial oxygen atoms obtained from single crystal neutron diffraction is due to the different thermal history of the samples or to the resolution related to different q-values for the two measurements. We note that the single crystal

data have been collected up to $\sin\theta/\lambda = 0.87$ Å^{-1}, whereas the NPD data are limited to $\sin\theta/\lambda = 0.71$ Å^{-1}.

As already reported for the average high-temperature tetragonal (HTT) *F4/mmm* structure of $Pr_2NiO_{4.23}$ at 400°C, significant anisotropic displacement factors were found for the apical and the equatorial oxygen atoms.[6] The anisotropy is almost four times larger along the *c*-axis for the equatorial oxygen atoms O(1) and O(2) while, for the apical O(3) atom, displacements are two times larger in the (*a*,*b*) plane compared to the *c*-axis. This has been reported for a series of K_2NiF_4 type oxides and is not only restricted to nickelates.[26, 27] These anisotropic displacements along [110] direction with respect to the F-cell, have been interpreted as dynamically activated libration-modes of the MO_6-octahedra, induced by the presence of interstitial oxygen atoms, pushing away the coordinating O_{ap} atoms, and thus creating an oxygen diffusion pathway along the [110]-direction inside the Pr_2O_2 rock-salt layer, towards the interstitial sites.[6, 8, 28, 29] A similar behaviour is also evidenced here by the Maximum Entropy reconstruction of the nuclear densities for the $Pr_2NiO_{4.09}$ phase, due to the presence of O_{int}.

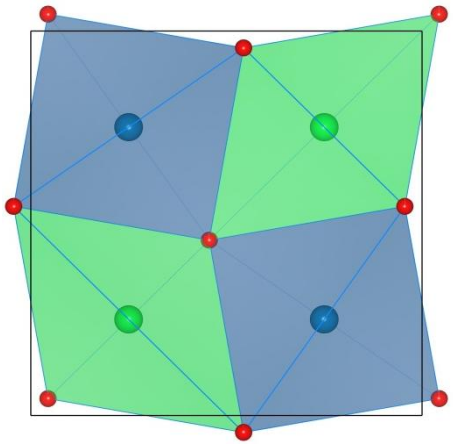

Figure 6. The two different tetrahedral sites with *4b* (green) and *4e* (blue) Wykoff notation showing *2.mm* and $\bar{4}$ site symmetry respectively. The *4b* tetrahedra are rotated by 10° around the *c*-axis.

The phased data obtained for $Pr_2NiO_{4.09}$ from neutron diffraction were used for the reconstruction of the scattering densities by the maximum entropy method (MEM), giving the most probable unconstrained and unbiased scattering distribution. This is equivalent to an anharmonic description of all constituents, which is model free, the only constraint being the symmetry given by the space group. The MEM approach has also the advantage to consider strong and weak reflections with equal importance, resulting in a much better defined background in the nuclear scattering maps compared to the classical Fourier-methods, particularly interesting when the description of the extra oxygen atoms or some disorder is needed.

The nuclear density distribution of $Pr_2NiO_{4.09}$ obtained by MEM is reported in Figure 7, where sections from $0.16 \leq z \leq 0.34$ clearly evidence the influence of the interstitial oxygen atoms on the displacements of the coordinating O_{ap} atoms. In addition to their equilibrium positions, extra nuclear scattering densities become evident in a way that all four coordinating apical oxygen atoms around an O_{int} are pushed away, implying a symmetrical increase of the $O_{int}(O_{ap})_4$

polyhedron at least on a local scale. We note, however, that the selective (4b) tetrahedral site occupation is only 10%, not allowing a cooperative long-range order of the $O_{int.}$ The increase for the partially occupied (4b) tetrahedra goes along with the reduction of the other remaining tetrahedra in the unit cell, reflecting both displacement directions of the O_{ap} as confirmed by the MEM data. The displacements of all apical oxygen atoms are thus highly anharmonic, putting a general problem on classical structure refinement using harmonic displacement ellipsoids. This, consequently, allows understanding the refinement qualities (see Table 1) resulting in an R-factor above 5%, while the R_{int} of 2.8 % confirms the excellent data quality of the measured intensities.

The steric effects due to the presence of the interstitial oxygen atoms here is thus completely equivalent to the behaviour found for the displacements of the apical oxygen atoms in $Pr_2NiO_{4.23}$, following an intersticialcy push-pull diffusion mechanism, as found for K_2NiF_4 type oxides but commonly occurring at more elevated temperatures.[8, 30]

Beside a better structural understanding of the intermediate phase with respect to the oxygen diffusion mechanism, we also checked for possible magnetic reflections such as (100)/(101)/(011), as reported for $Pr_2NiO_{4.06}$.[31] In agreement with the powder diffractograms obtained during the *in situ* studies reported above, we confirm the absence of these reflections confirming the absence of any magnetic ordering at ambient T.

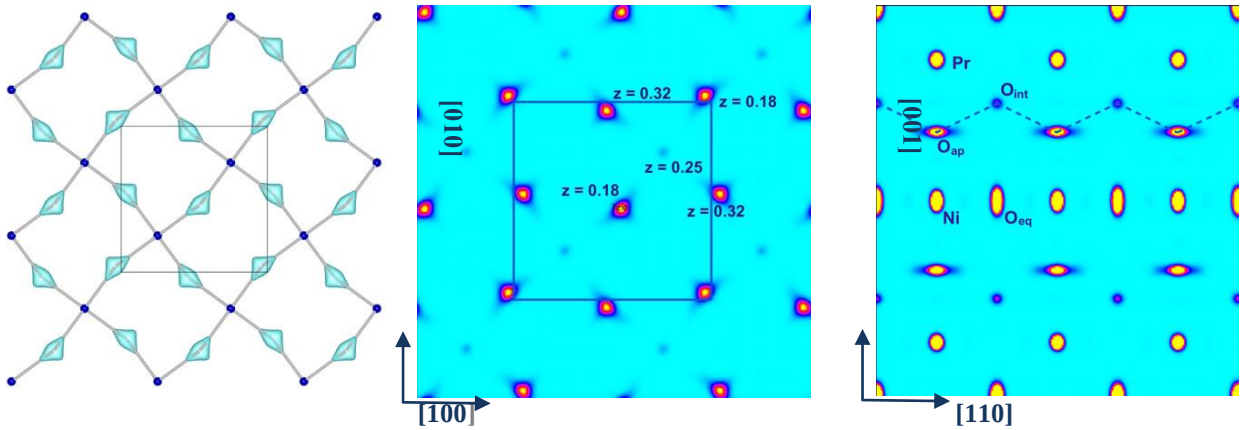

Figure 7. Illustration of the anharmonic displacements of the apical oxygen atoms inside the Pr_2O_2 rock-salt layer, as reconstructed by the MEM method. Left: isosurfaces of the O_{ap} (green) tetrahedrally coordinated by O_{int} atoms (blue). Middle: projection of the nuclear densities for $0.16 \leq z \leq 0.34$; the *F*-unit cell is outlined. Right: [110]/[001] projection cut along [1-10] with an integration thickness $\Delta_{(x,x)} = 0.07$ showing the oxygen diffusion pathway along [110], outlined with a blue dashed line.

4. Conclusion

The electrochemical reduction in aqueous alkaline electrolyte and subsequent oxidation of as sintered $Nd_2NiO_{4.24}$ and $Pr_2NiO_{4.23}$ electrodes appear to be very similar for both compounds in terms of structural evolution with the charge transfer. In both cases, a two-phase reaction step transforms the starting phases into a non-stoichiometric tetragonal phase ($0.07 \leq \delta \leq 0.10$), which subsequently transforms, again in a two-phase reaction, into the respective stoichiometric $RE_2NiO_{4.00}$ phases. The oxidation processes are, however, significantly different, showing tetragonal $Nd_2NiO_{4.10}$ and orthorhombic $Pr_2NiO_{4.17}$ as the maximum re-oxidised phases, while reaching oxygen gas formation at the electrode. It seems that, in both cases, the phases with the maximum possible oxygen stoichiometry, corresponding to $\delta = 0.24$ for PNO and $\delta = 0.23$ for

NNO, are avoided. One explanation for this not fully reversible oxidation might originate from the extra strain, necessary to induce a monoclinic distortion and associated formation of oxygen ordering, as described in ref.[6].

It is thereby intriguing to see that the phase diagram obtained by electrochemical reactions at ambient temperature is essentially corresponding to the phases obtained by classical solid-state reactions under controlled oxygen partial pressure at high temperatures. In this context, it is remarkable to observe that a selective occupation of only one out of two tetrahedral sites is achieved during the formation of the tetragonal intermediate phase. The formation mechanisms and stability for these phases, showing a narrow composition range of $0.07 \leq \delta \leq 0.10$, are not clear yet. Electrochemical cycling of structurally closely related $La_2CuO_{4+\delta}$ and $La_2CoO_{4+\delta}$ only shows orthorhombic symmetry for $\delta_{max} = 0.07$ and 0.25 respectively, while $La_2NiO_{4.0}$ becomes tetragonal for already small values of δ.[32, 33] It is clear that we are still far away from an understanding of the subtle structural deformations induced by small changes in δ values in Ruddlesden-Popper type oxides. It would be of particular interest to explore oxygen intercalation reactions in non-aqueous electrolytes, allowing to significantly increase both reduction and oxidation potentials, and presumably allowing to access higher oxygen doping concentrations.

ASSOCIATED CONTENT

Supporting Information.

The following files are available free of charge.

Additional diffraction data and refinements results (PDF)

AUTHOR INFORMATION

Corresponding Author

monica.ceretti@umontpellier.fr

Author Contributions

The manuscript was written through contributions of all authors. All authors have given approval to the final version of the manuscript.

Funding Sources

This work was financially supported by the French National Agency Research ANR projects "Assisted Mechanisms for Oxygen Ionic conduction in non-Stoichiometric oxides" (AMOXIS, No. ANR-14-CE05-0016-02) and "Structural induced Electronic Complexity controlled by low temperature Topotactic Reaction" (SECTOR No. ANR-14-CE36-0006-01).

ACKNOWLEDGMENT

We would like to thank Dr. F. Porcher of the Laboratoire Léon Brillouin (LLB, Saclay, France) for having given us the possibility to perform a data collection on the 3T2 diffractometer. X-rays diffraction measurements have been performed at the "Plateforme d'Analyse et de Caractérisation du Pôle Chimie Balard", Montpellier, France. Single crystal neutron diffraction data have been measured at the single crystal diffractometer HEiDi operated jointly by RWTH Aachen and Forschungszentrum Jülich GmbH (JARA cooperation) at the Heinz Maier-Leibnitz Zentrum (MLZ, Garching, Germany).

REFERENCES

1. Kovalevsky, A. V.; Kharton, V. V.; Yaremchenko, A. A.; Pivak, Y. V.; Tsipis, E. V.; Yakovlev, S. O.; Markov, A. A.; Naumovich, E. N.; Frade, J. R. Oxygen permeability, stability and electrochemical behavior of $Pr_2NiO_{4+\delta}$ -based materials. *J. Electroceram.* **2007,** 18, 205-218.
2. Takahashi, S.; Nishimoto, S.; Matsuda, M.; Miyake, M. Electrode Properties of the Ruddlesden–Popper Series, $La_{n+1}Ni_nO_{3n+1}$ (n=1, 2, and 3), as Intermediate-Temperature Solid Oxide Fuel Cells. *J. Am. Ceram. Soc.* **2010,** 93, 2329-2333.
3. Ishihara, T. Oxide ion conductivity in defect perovskite, Pr_2NiO_4 and its application for solid oxide fuel cells. *Journal of the Ceramic Society of Japan* **2014,** 122, 179-186.
4. Perrichon, A.; Piovano, A.; Boehm, M.; Zbiri, M.; Johnson, M.; Schober, H.; Ceretti, M.; Paulus, W. Lattice Dynamics Modified by Excess Oxygen in $Nd_2NiO_{4+\delta}$: Triggering Low-Temperature Oxygen Diffusion. *J. Phys. Chem. C* **2015,** 119, 1557-1564.
5. Paulus, W.; Schober, H.; Eibl, S.; Johnson, M.; Berthier, T.; Hernandez, O.; Ceretti, M.; Plazanet, M.; Conder, K.; Lamberti, C. Lattice Dynamics To Trigger Low Temperature Oxygen Mobility in Solid Oxide Ion Conductors. *J. Am. Chem. Soc.* **2008,** 130, 16080-16085.
6. Ceretti, M.; Wahyudi, O.; Cousson, A.; Villesuzanne, A.; Meven, M.; Pedersen, B.; Bassat, J. M.; Paulus, W. Low temperature oxygen diffusion mechanisms in $Nd_2NiO_{4+\delta}$ and $Pr_2NiO_{4+\delta}$ via large anharmonic displacements, explored by single crystal neutron diffraction. *J. Mater. Chem. A* **2015,** 3, 21140-21148.
7. Paulus, W.; Cousson, A.; Dhalenne, G.; Berthon, J.; Revcolevschi, A.; Hosoya, S.; Treutmann, W.; Heger, G.; Le Toquin, R. Neutron diffraction studies of stoichiometric and oxygen intercalated La_2NiO_4 single crystals. *Solid State Sciences* **2002,** 4, 565-573.
8. Parfitt, D.; Chroneos, A.; Kilner, J. A.; Grimes, R. W. Molecular dynamics study of oxygen diffusion in $Pr_2NiO_{4+\delta}$. *Phys. Chem. Chem. Phys.* **2010,** 12, 6834-6836.
9. Villesuzanne, A.; Paulus, W.; Cousson, A.; Hosoya, S.; Le Dreau, L.; Hernandez, O.; Prestipino, C.; Houchati, M. I.; Schefer, J. On the role of lattice dynamics on low-temperature oxygen mobility in solid oxides: a neutron diffraction and first-principles investigation of $La_2CuO_{4+\delta}$. *J. Solid State Electrochem.* **2011,** 15, 357-366.
10. Li, X.; Benedek, N. A. Enhancement of Ionic Transport in Complex Oxides through Soft Lattice Modes and Epitaxial Strain. *Chem. Mater.* **2015,** 27, 2647-2652.
11. Bhavaraju, S.; DiCarlo, J. F.; Scarfe, D. P.; Yazdi, I.; Jacobson, A. J. Electrochemical Intercalation of Oxygen in Nd_2NiO_{4+x} ($0 < x < .0.18$) at 298 K. *Chem. Mater.* **1994,** 6, 2172-2176.
12. Le Toquin, R.; Paulus, W.; Cousson, A.; Prestipino, C.; Lamberti, C. Time-resolved in situ studies of oxygen intercalation into $SrCoO_{2.5}$, performed by neutron diffraction and X-ray absorption spectroscopy. *J. Am. Chem. Soc.* **2006,** 128, 13161-13174.
13. Wahyudi, O.; Ceretti, M.; Weill, I.; Cousson, A.; Weill, F.; Meven, M.; Guerre, M.; Villesuzanne, A.; Bassat, J. M.; Paulus, W. Growth of high quality single crystals of strontium doped (Nd,Pr)-nickelates, $Nd_{2-x}Sr_xNiO_{4+\delta}$ and $Pr_{2-x}Sr_xNiO_{4+\delta}$ *Crystengcomm* **2015,** 17, 6278-6285.
14. Rodríguez-Carvajal, J. Recent developments of the program FullProf. Commission for Powder Diffraction. *IUCr Newsletter* **2001,** 26, 12-19. The complete FULLPROF suite can be obtained from: http://www.ill.eu/sites/fullprof/index.html.
15. Sheldrick, G. A short history of SHELX. *Acta Crystallographica Section A* **2008,** 64, 112-122.
16. F. Izumi , R. A. D. *Recent Research Developments in Physics*; 81-7895-046-4; **2002**; pp 699-726.

17. Momma, K.; Izumi, F. VESTA 3 for three-dimensional visualization of crystal, volumetric and morphology data. *J. Appl. Crystallogr.* **2011,** 44, 1272-1276.
18. Zaghrioui, M.; Giovannelli, F.; Brouri, N. P. D.; Laffez, I. Anomalies in magnetic susceptibility of nonstoichiometric $Nd_2NiO_{4+\delta}$ (δ=0.049, 0.065, 0.077, 0.234). *J. Solid State Chem.* **2004,** 177, 3351-3358.
19. Ishikawa, K.; Metoki, K.; Miyamoto, H. Orthorhombic–orthorhombic phase transitions in $Nd_2NiO_{4+\delta}$ ($0.067 \leq \delta \leq 0.224$). *J. Solid State Chem.* **2009,** 182, 2096-2103.
20. Ishikawa, K. Crystal structure of $Nd_2NiO_{4.08}$. *Solid State Ionics* **2014,** 262, 682-686.
21. Fernández-Díaz, M. T.; Rodríguez-Carvajal, J.; Martínez, J. L.; Fillion, G.; Fernández, F.; Saez-Puche, R. Structural and magnetic phase transitions in Pr_2NiO_4. *Z. Physik B - Condensed Matter* **1991,** 82, 275-282.
22. Fernández-Díaz, M. T.; Martínez, J. L.; Rodríguez-Carvajal, J. High-temperature phase transformation of oxidized $R_2NiO_{4+\delta}$ (R=La, Pr and Nd) under vacuum. *Solid State Ionics* **1993,** 63–65, 902-906.
23. Fernandez Diaz, M. T.; Martinez, J. L.; Rodriguez Carvajal, J.; Beille, J.; Martinez, B.; Obradors, X.; Odier, P. Metamagnetism in Single-Crystal Pr_2NiO_4. *Phys Rev B* **1993,** 47, 5834-5840.
24. Fernández-Díaz, M. T.; Rodríguez-Carvajal, J.; Martínez, J. L.; Odier, P. Low temperature phase and magnetic ordering in Pr_2NiO_4. *Physica B: Condensed Matter* **1992,** 180–181, Part 1, 122-124.
25. Sullivan, J. D.; Buttrey, D. J.; Cox, D. E.; Hriljac, J. A Conventional and High-Resolution Synchrotron X-Ray-Diffraction Study of Phase Separations in $Pr_2NiO_{4+\delta}$. *J. Solid State Chem.* **1991,** 94, 337-351.
26. Le Toquin, R.; Paulus, W.; Cousson, A.; Dhalenne, G.; Revcolevschi, A. Interstitial and apical oxygen order–disorder in $La_2CoO_{4+\delta}$ observed by single-crystal neutron and X-ray diffraction. *Physica B: Condensed Matter* **2004,** 350, E269-E272.
27. Le Dréau, L.; Prestipino, C.; Hernandez, O.; Schefer, J.; Vaughan, G.; Paofai, S.; Perez-Mato, J. M.; Hosoya, S.; Paulus, W. Structural Modulation and Phase Transitions in $La_2CoO_{4.14}$ Investigated by Synchrotron X-ray and Neutron Single-Crystal Diffraction. *Inorg. Chem.* **2012,** 51, 9789-9798.
28. Yashima, M.; Enoki, M.; Wakita, T.; Ali, R.; Matsushita, Y.; Izumi, F.; Ishihara, T. Structural Disorder and Diffusional Pathway of Oxide Ions in a Doped Pr_2NiO_4-Based Mixed Conductor. *J. Am. Chem. Soc.* **2008,** 130, 2762-2763.
29. Yashima, M.; Sirikanda, N.; Ishihara, T. Crystal Structure, Diffusion Path, and Oxygen Permeability of a Pr_2NiO_4-Based Mixed Conductor $(Pr_{0.9}La_{0.1})_2(Ni_{0.74}Cu_{0.21}Ga_{0.05})O_{4+\delta}$. *J. Am. Chem. Soc.* **2010,** 132, 2385-2392.
30. Chroneos, A.; Parfitt, D.; Kilner, J. A.; Grimes, R. W. Anisotropic oxygen diffusion in tetragonal $La_2NiO_{4+\delta}$: molecular dynamics calculations. *J. Mater. Chem.* **2010,** 20, 266-270.
31. Buttrey, D. J.; Sullivan, J. D.; Shirane, G.; Yamada, K. Influence of oxygen nonstoichiometry on structure and magnetism in $Pr_2NiO_{4+\delta}$. *Phys Rev B* **1990,** 42, 3944-3951.
32. Paulus, W. Etude de l'intercalation et du désordre de l'oxygène dans quelques oxydes de basse dimension. Université Paris XI, Orsay, 1998.
33. Paulus, W.; Heger, G.; Rudolf, P.; Schöllhorn, R. In situ neutron diffraction studies on the electrochemical oxidation of polycrystalline La_2CuO_4. *Physica C: Superconductivity* **1994,** 235-240, 861-862.

For Table of Contents Only. Structural evolution of $(Pr/Nd)_2NiO_{4+\delta}$ electrodes was followed by *in situ* neutron diffraction during electrochemical reaction, as a function of oxygen stoichiometry.